

RADON FLUX DENSITY IN CONDITIONS OF PERMAFROST THAWING: SIMULATION EXPERIMENT

Andrey V. Puchkov^{1*}, Elena V. Berezina², Evgeny Yu. Yakovlev¹, Nicholas R. Hasson³, Sergey V. Druzhinin¹, Alexey S. Tyshov¹, Ekaterina V. Ushakova⁴, Lev S. Koshelev¹, Pavel I. Lapikov¹

¹N. Laverov Federal Centre for Integrated Arctic Research of the Ural Branch of Russian Academy of Sciences, 109 Severnoy Dviny Emb., Arkhangelsk, 163000, Russia.

²A.M. Obukhov Institute of Atmospheric Physics, Russian Academy of Sciences, 119017 Moscow, Russia

³Water and Environmental Research Center, University of Alaska Fairbanks, 1764 Tanana Loop, Fairbanks, AK 99775, USA

⁴Yuri Gagarin State Technical University of Saratov, 77 Politechnicheskaya street, Saratov, 410054, Russia.

*Corresponding author: andrey.puchkov@fciaarctic.ru

Received: March 6th, 2022 / Accepted: August 8th, 2022 / Published: October 1st, 2022

<https://DOI-10.24057/2071-9388-2022-023>

ABSTRACT. This paper describes a five-month experiment (February – July 2021) measuring the gradual thaw diffusion of radon-222 (further in the article – radon) from a frozen environment in NW Russia (i.e. Arkhangelsk region). Red clay substrate containing a high content of ²²⁶Ra filled the bottom insides of 200-liter barrel holding the source of radon and buried at 1.6 m depth (e.g., the radium source zone), then covered with native soil, filled with water and frozen under in-situ conditions. Radon measurements were carried out from soil surface above the container (disturbed soil layer) and at background location (undisturbed soil layer). Several periods of increased radon flux density were observed, which was related to radium source zone thawing. It was shown that in 1-2 days after thawing of the radium source zone and drying of the upper soil layer, the radon flux increases sharply – more than 8 times compared to background values. These results show a strong relationship between radon flux density and soil temperature profiles at different depths. The calculations of radon sourced from frozen and thawed zones show how temperature phase of substrate (e.g. clays) control the barrier influence of radon migration. It reduced them by 10-20 times (according to the results of a theoretical calculation), depending on the characteristics of frozen rocks (density, porosity). Thus, the barrier function of permafrost is related to the physical properties of ice and frozen rocks. These temperature phases controls radon emanation coefficients and significantly influences the migration of radon to the earth's surface.

KEYWORDS: Radon hazard, permafrost, Arctic, climate warming, natural radioactivity, frozen soil

CITATION: Puchkov A. V., Berezina E. V., Yakovlev E. Yu., Hasson N. R., Druzhinin S. V., Tyshov A. S., Ushakova E. V., Koshelev L. S., Lapikov P. I. (2022). Radon Flux Density In Conditions Of Permafrost Thawing: Simulation Experiment. *Geography, Environment, Sustainability*, 3(15), 5-18

<https://DOI-10.24057/2071-9388-2022-023>

ACKNOWLEDGEMENTS: This work was supported by the grant of the Russian Science Foundation No 20-77-10057 (preparation of the research site and the object of study, calculation of the radiation and physical parameters of the object of study, assessment of the emanation coefficient and the radon production rate in soils), the grant of the Project Office For Arctic Development No. 245G dated 04/19/2021 (measurement and analysis of radon flux density at control and background points, soil temperatures at different depths, calculation of the diffusion model) and the grant of the Ministry of Science and Higher Education of Russia No 075-15-2021-934 (statistical and factor analysis of changes in radon flux density under experimental condition).

Conflict of interests: The authors reported no potential conflict of interest.

INTRODUCTION

Over the past few years, the problem of climate change has grown to be the most pressing issue in the world. As the arctic regions warm twice the global rate, changes in the relief, vegetation, fauna and property intensify (Zolkos et al. 2021). Rapid thawing leads to distinct ground collapse and high topographical relief, leading to thermokarst wetlands that further accelerate thawing by increasing talik formation and wetland development (Farquaharson et al. 2019).

One of the most important negative results of climate warming is the thawing of permafrost soils. Thermokarst

wetlands and abrupt thawing promote greenhouse gas (GHG) emissions of carbon dioxide (CO₂) and methane (CH₄), which in turn accelerate polar amplification, which promote further ground thaw/collapse, and leading to a potential permafrost carbon feedback. (Walter Anthony et al. 2018; Obu et al. 2019, Biscaborn et al. 2019). Recent studies indicated that the permafrost boundary is gradually shifting from south to north and its depth is progressively increasing (Zhang et al. 2021). Few examples of such behaviors are noticeable such as the giant sinkhole-blow out craters in the Yamalo-Nenets Autonomous Okrug (Buldovicz et al. 2018), the collapse of major industrial buildings in Norilsk (Koptev 2020) and rapid relief changes in

the boreal and/or tundra ecosystems (Ji et al. 2019, Doloisio et al. 2020).

While changes in the parameters of permafrost leads to the redistribution of macro- and microelements in the geological environment (Shirokova 2021, Dahédrey Payandi-Rolland 2021, Pokrovsky 2021), one poorly understood factor has so far remained underdeveloped here but is related to the afermomednted permafrost degradation processes – natural radioactivity – which everywhere in the geological environment, including landforms developed under permafrost conditions. Our prior work concerning radioactivity and the radioactive radon gas emerging from permafrost provides the justified context for these above concerns, as we investigated both the policy and shortfalls of environmental monitoring of radioactive elements in permafrost settings (Puchkov et al. 2021).

Radon is a member of the uranium-238 radioactive decay chain, which makes up over 99% of all uranium on earth. Radon is constantly formed in all geological environments. The physical and chemical properties of radon allow it to be used as a tracer for studying many geological and atmospheric processes (Sabbarese et al. 2021, Giustini et al. 2019, Miklyaev et al. 2010, Baskaran et al. 2016, Daraktchieva et al. 2021, Selvam et al. 2021). At the same time, radon is a dangerous radioactive element that can lead to lung cancer where high concentrations are present, for example, in dwellings (Lorenzo-Gonzalez et al. 2020, Maier et al. 2021, Petrova et al. 2020, Rodríguez-Martínez et al. 2018, Rosenberger et al. 2018).

Until now, there are few scientific works devoted to the behavior of radon in frozen rocks and permafrost, while at the same time thawing and changing phase boundaries, thereby altering the pathways for radon migration to the surface. Most of those works are of a theoretical nature (Puchkov et al. 2021). Technically, there is existing scientific works showing permafrost is an excellent barrier to migiate upward migration of radon from the ground (Glover et al. 2022) which shows the need to extend these results elsewhere, as permafrost conditions are heterogenous and geographically unique. This concerns drives our investigations into how radioactive gas will migrate and to flow to the earth surface if permafrost thaws.

The purpose of this scientific paper is to demonstrate the influence of the process of thawing of frozen soils on radon flux during a laboratory experiment. For this, an experimental site with a frozen container containing ²²⁶Ra (radioactive source) was prepared. The total activity of the radioactive source was about 4200 Bq and the radon flux density (RFD) was measured over a 5-month period. These experimental results will contribute to the fate and transport of radon emissions from permafrost to post-permafrost conditions.

MATERIALS AND METHODS

The experimental site is located in the Arkhangelsk region (NW Russia), 30 km from the city of Severodvinsk (Fig. 1). This territory belongs to the northern part of the East European plain. The region is characterised by a glacially formed landscape of flat plains, laterally extensive terraces and moraine belts dissected by river valleys (Jensen 2009). At the experimental site, the overburden layer is made of a mixture of gley-podzolic soils and loams, that is typical for this territory and the northern taiga. The upper soil layers were exposed to anthropogenic impacts after its agricultural use making them mix layers (urban soils). The content of ²²⁶Ra in these soils is low and equal to about 10 Bq·kg⁻¹. For this reason, the background radon flux did not interfere with the experiment. Site and container preparations were carried out in February 2021. During this period, the air temperature reached -40°C. A red clay with an increased content of ²²⁶Ra was used as a source of radon. Detailed radiation and physical characteristics of the radon source and the «background» soils are presented. During 5 months (March – July 2021, n days = 132), the RFD was measured in the control and background points coupled with soil temperature of 0.5, 1.0 and 1.5 m depths. The average daily temperatures at the city of Arkhangelsk, Russia according to the Northern Directorate for Hydrometeorology and Environmental Monitoring (<http://www.sevmeteo.ru/>) was used as the temperature of the atmospheric air.

Experimental site

The experimental setup uses a container placed in a pit of 1.6 m deep. The height of the container is 86 cm. The bottom inside container holds 40 kg of red clay (e.g radium source zone). The radium source zone was covered with surrounding soil up to the top of the container (overlapping layer). Holes were drilled at the bottom of the container for drainage of melt water. A detailed diagram of the experimental setup, its location and geometric characteristics are shown in Fig. 1. The container was then filled with water daily and reached a volume of 50 liters for 7 days (total 350 liters of water). We specially prepared more water in the container because some of the water went through the drainage holes and also through the top of the container, allowing it to freeze on all sides of the outside. In extremely low temperatures (down to -40°C), the content of the container was quickly and naturally frozen. After freezing is achieved by temperature logger observations, the pit was backfilled with prior in-situ soil. Thus, the frozen container and prior soils filled the exgivated pit.

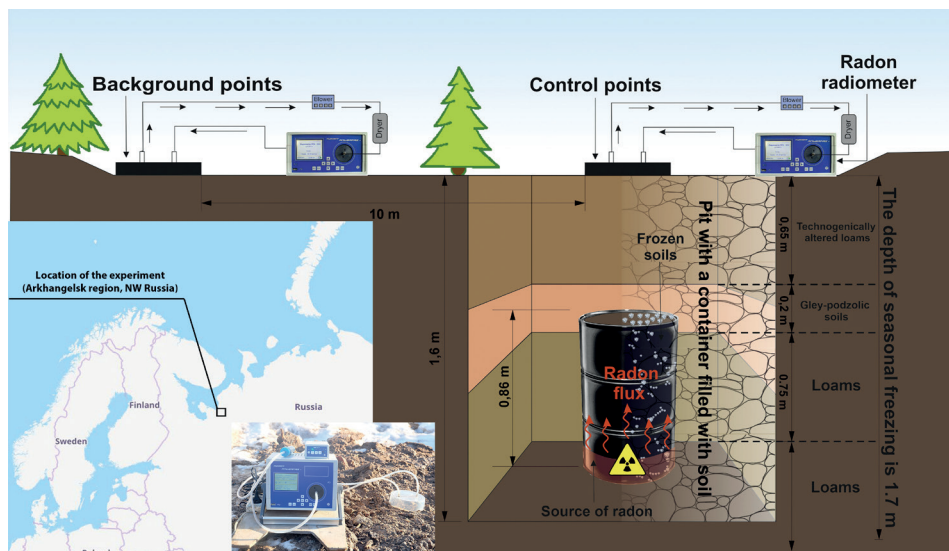


Fig. 1. The location of the experimental site and its geometric characteristics

Measurements of the RFD were carried out at two points. The control point was above the container and the background point was also at the surface at 10 meters away from the control point. When the topsoil subsided under thawing conditions, soils were added so that the measurement height above control point of the measurement did not change.

Radiometric measurement method

The measurement of the RFD using the radon radiometer «Alpharad plus» (Manufacturer – «NTM» Protection, Moscow city, Russia) (Fig. 2) is based on the electrostatic deposition of charged ^{218}Po ions from the air sample to the surface of the semiconductor detector. The electrical impulses generated by alpha particles on the detector were amplified with a preamplifier, fed to the input of an analogue-to-digital converter and then processed with a computer. The measurements were displayed on a colour LCD screen and stored in a non-volatile memory. The radon radiation was determined by the number of registered alpha particles during the decay of ^{218}Po atoms deposited on the detector (Afonin 2013).

The samplers were installed on a leveled ground. The sampler is made of plastic. The depth of immersion in the soil is 1 cm. The edges of the sampler were covered with soil to prevent contact with the atmosphere. The sampler was stored for 30 minutes to allow radon accumulation. Air was then pumped through the radiometer chamber for 20 minutes. The measurement was carried out twice for 20 minutes. Before the second measurement, air was pumped again through the radiometer chamber. About 2 hours are necessary between the moment the sampler is installed and the measurement is obtained. Since the measurements were carried out at two points (background and control), two radon radiometers of the same type were used. A reference sample was initially used to test the convergence of the measurements using the two radiometers. The relative standard deviation of the measurements from the reference sample was no more than

5-8%. As a reference sample, a 5-liter container with granite having a ^{226}Ra activity of about $95 \text{ Bq}\cdot\text{kg}^{-1}$ and an emanation rate of 15% was used.

Gamma Spectrometry Measurements

Gamma spectrometry is a widely used method to measure gamma radiation from radionuclides of natural origin, including Ra-226. It is a universal, non-destructive and easy-to-use method, especially at the stage of sample preparation and in the measurement process (Syam et al. 2020, IAEA 2013). A semiconductor gamma-spectrometric complex with nitrogen cooling ORTEC with a GEM 10 P4-70 HPGe detector (Ametek Ortec, Oak Ridge, TN, USA) complete with lead shielding was used to determine radionuclide Ra-226 in soils and radium source zone. The gamma spectrometer resolution along the 1.33 MeV (^{60}Co) line is 1.75 keV and its relative efficiency is 15%. The measurement geometry is a 1-L Marinelli vessel (counting sample). The activity of the Ra-226 radionuclide is determined from the radionuclide Pb-214 (351.93 keV with a quantum yield of 35.60%) and Bi-214 (609.32 keV with a quantum yield of 45.49%, 1120.29 keV with a quantum yield of 14.92%, 1764.49 keV yield with a quantum yield of 15.3%).

Calculation methods

The radon emanation coefficient can be determined by two methods: gamma-spectrometric and radiometric (emanation) methods. The gamma spectrometric method was selected for the present research. The method consists of measuring the gamma activity of samples at various intervals after they are placed in a hermetically sealed container. We used a Marinelli plastic container sealed with a thick layer of sealant. According to our experimental data (Yakovlev et al. 2021), this method of sealing allows minimizing radon leakage from the container. In this experiment, counting samples were prepared in the form of a crushed sample with a

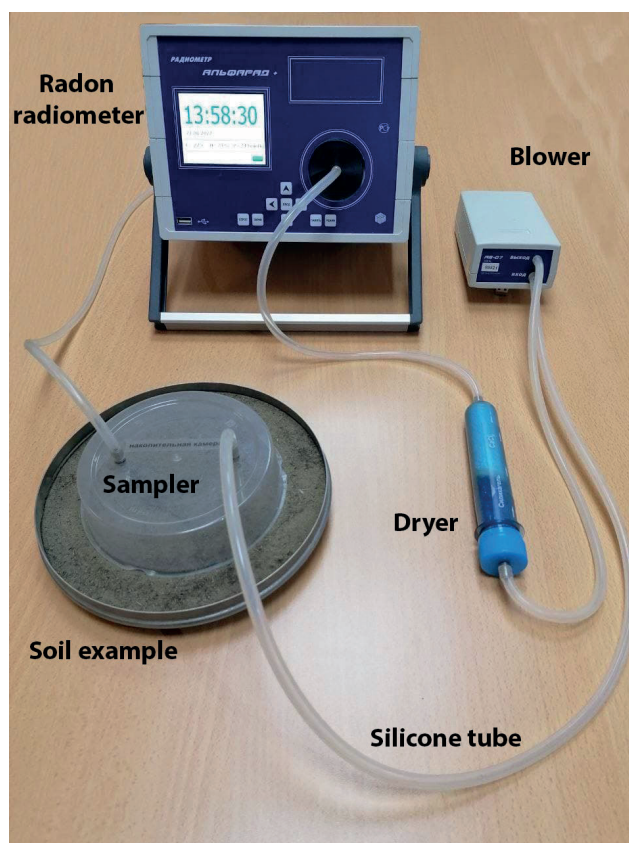


Fig. 2. The radon radiometer «Alpharad plus»

grain size of less than 0.5 mm in a 1-L Marinelli vessel. Samples were measured daily for 21 days after they were sealed. Based on the results of these measurements, the following were determined: the activity of ²²⁶Ra without taking into account the accumulation of its decay products; the activity of ²²⁶Ra taking into account the accumulation of its decay products; the emanation coefficient; and the period during which the daughter products of ²²⁶Ra decay enter a state of radioactive equilibrium. The counting sample was depressurized after the experiment and after 1–2 days for the activity of ²²⁶Ra to be measured again. Based on the results of the experiment, the radon emanation coefficient (its free state) was determined using the following equation (1):

$$KRn = \left(1 - \frac{A_{226Ra} (non-equilibrium)}{A_{226Ra} (equilibrium)} \right) \times 100 \quad (1)$$

where $A_{226Ra} (non-equilibrium)$ is the activity of ²²⁶Ra (in a nonequilibrium state) determined as the average value of the results of the first and last measurements (unsealed) in Bq·kg⁻¹; and $A_{226Ra} (equilibrium)$ is the specific activity of ²²⁶Ra (in an equilibrium state) determined as the average value of the results of the last 5 measurements in a sealed state, in Bq·kg⁻¹.

The radon production rate, P (Bq·m⁻³·h⁻¹), was calculated using the following equation (2) (IAEA 2013, Pereira et al. 2017):

$$P = \lambda K_{Rn} A_{226Ra} \rho_b \quad (2)$$

where λ is the decay constant for radon (2.1·10⁻⁶ s⁻¹) and ρ_b is the bulk density, in kg·m⁻³.

The average density of the rock sample was determined by paraffin-coated method. This last physical parameter was calculated to assess the level of radon production. A detailed method and algorithm for calculating the average density are given in Yakovlev (2021) in which the average density of rock made of kimberlite was estimated.

RESULTS AND DISCUSSION

Radiation and physical parameters of soils and the radium source zone on the site

Table 1 shows the general characteristics of the samples under study. The studied soils are represented by the following: (1) technogenically altered loams, (2) gley-podzolic soils, (3) loams, (4) overlying soils (mixed gley-podzolic soils and loams) and (5) red clay (radium source zone). The background measurement points are represented by soils (1) – (3). The measurement reference points are represented by the overlying soils (4) and the radium source zone (5).

Despite the overlying soils above the radium source zone have a mass of about 400 kg and a total activity of ²²⁶Ra of about 4200 Bq, the low levels of emanation coefficient and radon production rate do not allow them to create high values of the RFD. This can be seen as the background point, i.e. at which the highest value of the RFD does not exceed 45 mBq·m⁻²·s⁻¹ (see Fig. 3). From table 1, it can be noted that the radium source zone has the highest values of the activity of ²²⁶Ra, the coefficient of emanation and the radon production rate.

Table 1. Radiation and physical parameters of soils and the radium source zone

| Type of soils | Radiation and physical parameters | | | |
|-------------------------------|--|--------------------------|--|----------------------------------|
| | ²²⁶ Ra concentration, Bq·kg ⁻¹ | Emanation coefficient, % | Radon production rate, Bq·m ⁻³ ·h ⁻¹ | Bulk density, g·cm ⁻³ |
| Technogenically altered loams | 10,9 | 10,3 | 12,7 | 1,5 |
| Gley-podzolic soils | 8,8 | 15,7 | 12,5 | 1,2 |
| Loams | 11,3 | 9,5 | 13,0 | 1,6 |
| Overlying soils | 10,4 | 12,2 | 14,4 | 1,5 |
| Red clay (radium source zone) | 103,8 | 25,7 | 322,7 | 1,6 |

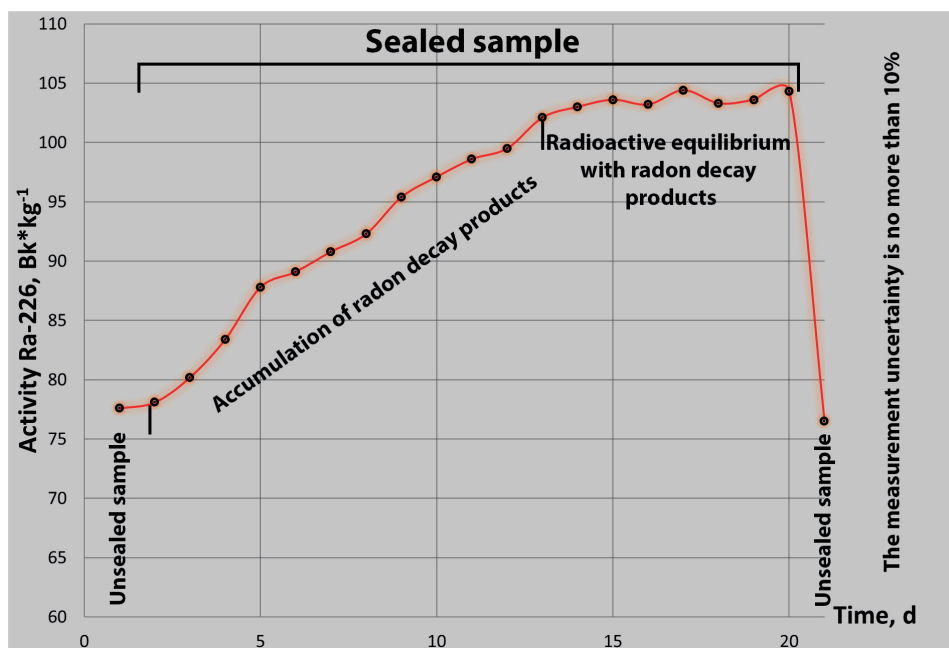


Fig. 3. The accumulation of radon decay products after sealing sample – red clay

The Fig. 3 shows an example of a curve for the accumulation of radon decay products after sealing sample – red clay. It can be noted that the state of radioactive equilibrium occurs in two weeks. The measurement uncertainty of ²²⁶Ra from its decay products was no more than 10%.

Seasonal changes in RFD

Changes in the RFD at the control and background points along with air and soil temperatures at different depths are shown in Fig. 4. From March 1 to July 11, an increase in the RFD occurred 4 times. The first time, the RFD increased slightly at the beginning of April, both at the control and background points. This is due to an increase in air temperature above 0°C and the beginning of thawing of the upper soil layers. In early May, when the air temperature sharply increased to 10-25 °C, the depth of soil thawing was up to 1 m. During this period, there was a second increase in the RFD. At the same time, the temperature of the radium source zone remained below 0°C. In this regard, the nature of the increase in the RFD was the same both for the control point and the background point. During this period, the depth of soil thawing continued to gradually increase. As soon as the surface temperature of the radium source zone increased to 0 °C and above, there was a sharp increase in the RFD at the control point. At the same time, at the background point, the radon activity did not change. From the moment the radium source zone began to thaw until its complete thawing, the RFD increased by about 7-8 times, reaching a maximum value of about 240 mBq·m⁻²·s⁻¹. Further, the radon activity did not change and the experiment was stopped afterward. Fluctuations in the RFD after complete thawing of the radium source zone were associated with weather events (rainfall) and changes in soil characteristics (moisture).

Statistical and factor analysis of changes in RFD under experimental conditions

Despite the dependence of the RFD on air and soil temperatures, a statistical analysis of the measured data was carried out and a correlation matrix was built. The statistical characteristics and the correlation matrix were divided into two large blocks (spring and summer) for convenience. Each block was divided into separate months. The results of the calculated statistical

characteristics and the correlation matrices are given in Appendix A.

There was a good correlation between air and soil temperature (R=0.73-0.89) as well as between RFD in control and background points (R=0.81) in March. In May, high relationships between air temperature and soil temperature at 0 meter (R=0.85) as well as between soil temperature at 0 m and 1 m (R=0.72) were observed. In April, there were no significant correlations in the measured parameters. This is due to the fact that the RFD varied only at the beginning of April and then the radon activity remained constant.

In spring, RFD changes were insignificant and were associated with thawing of soil up to 1.3 m deep. The RFD values at the control and background points during this period were the same, which means that there was no influence of the radium source zone. A significant correlation between RFDs in the control and background points were observed only in March (R=0.81) and in May (R=0.87) for the whole experiment.

The summer period (June) was characterized by a very good correlation between RFD at the control point and soil temperature at different depths (R=0.75 for 0 m, R=0.79 for 0.5 m, R=0.83 for 1.0 m, R=0.97 for 1.5 m). This is due to the fact that the radium source zone was intensely melting and contributed to an increase in RFD at the surface. At the same time, RFD at the background point remained at a constant level and no dependence on soil temperature was found.

Figs 5 and 6 show linear regressions for RFD and soil temperature at 1 m (for spring) and for RFD and soil temperature at 1.5 m (for summer). There is a good correlation (R=0.9) between radon flux density and soil temperature at 1 m depth in spring (Fig. 5) and at 1.5-m depth in summer (Fig. 6) at the control point. RFD increased by a factor of 26.7 and 22.2 in spring and in summer. This corresponds when soil temperature at 1-1.5-meter depth increased by 1 °C.

The calculated correlation matrices were approved by the construction of the frequency diagrams. Frequency distribution of RFDs in the control and background points (Fig. 7) is similar in March (up to 90% of RFDs in the range of 0.5-9 mBq/m²s and 0.5-5.5 mBq/m²s in the control and background points respectively) and in April (up to 90% of RFDs in the range of 12-18.5 mBq/m²s and 12-16.5 mBq/m²s in the control and background points respectively).

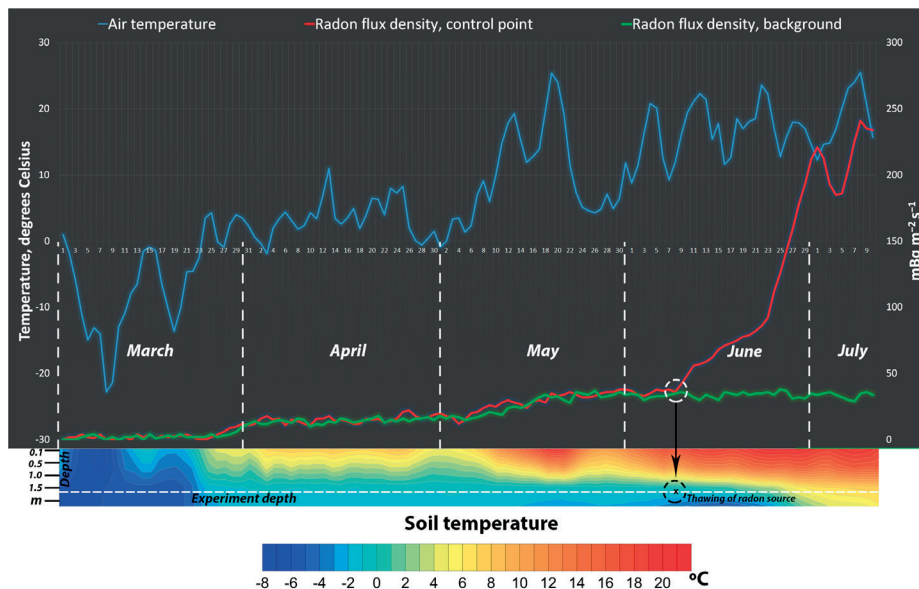


Fig. 4. Temporal changes in the RFD at the control and background points

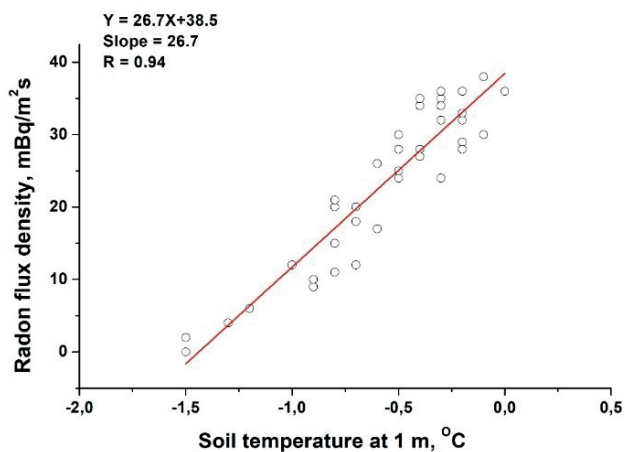


Fig. 5. Linear regression fits for RFD to soil temperature at 1 m depth from spring measurements in the control point

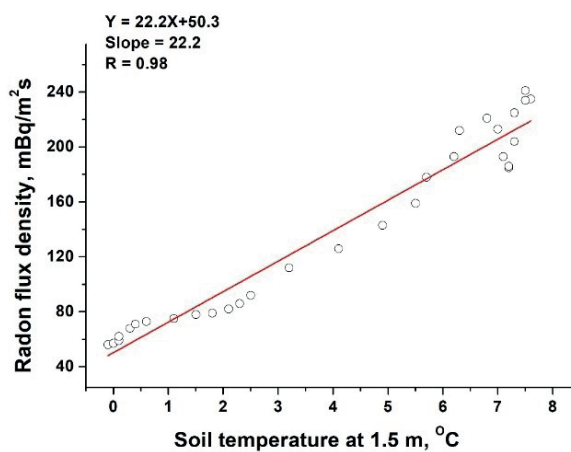


Fig. 6. Linear regression fits for RFD to soil temperature at 1.5 m depth in summer

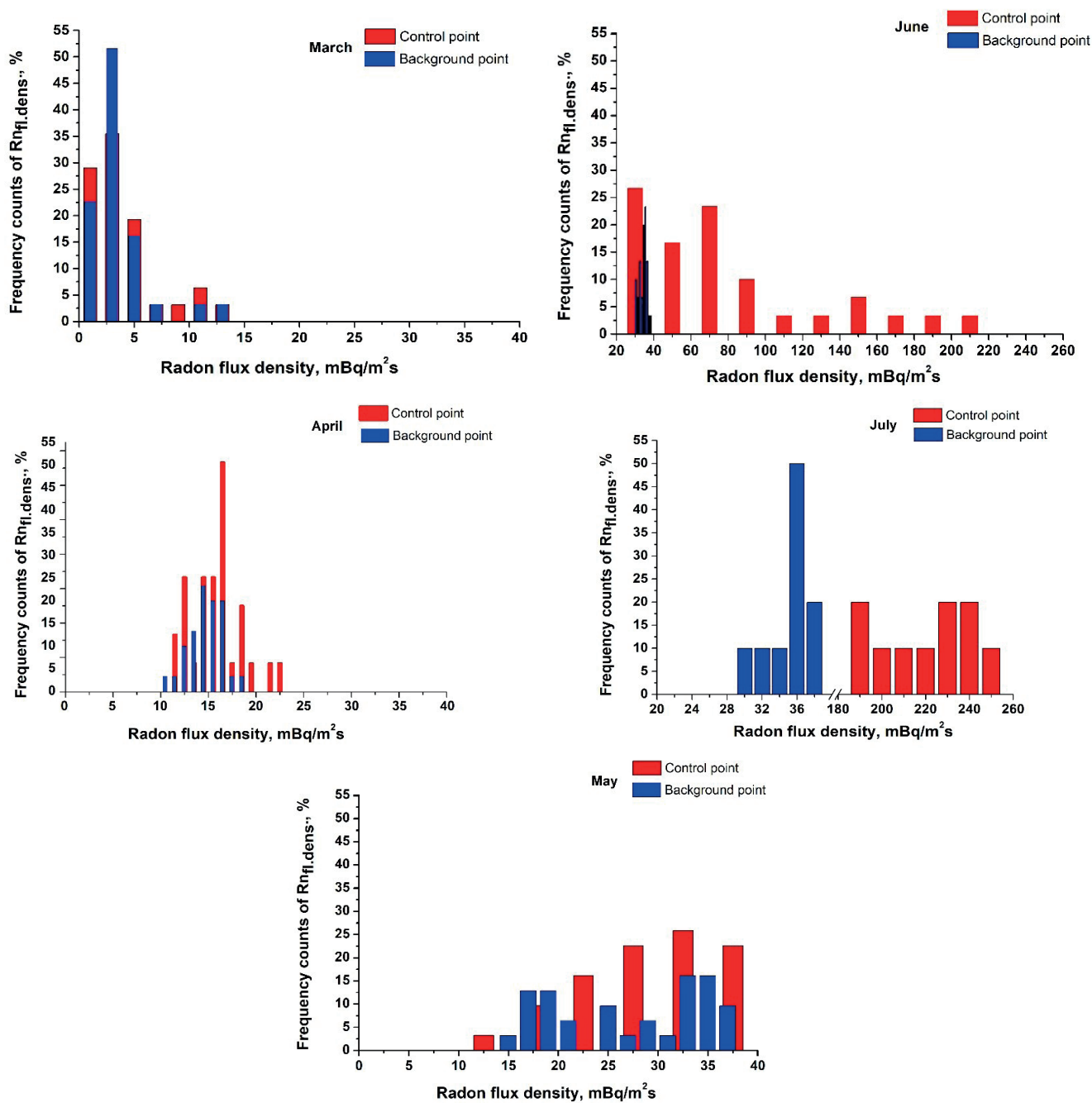


Fig. 7. Frequency counts (in %) of RFD for control (red) and background (blue) points

In May, RFDs in control and background points are about 2 times higher than in April.

In June and July, the significant difference (2-4 times) in RFDs between measurement points was observed. RFD in July in the control point reaches 238 mBq/m²s (90-th percentile) while RFD in the background point is 36 mBq/m²s (90-th percentile).

The factor analysis was used to select the main factor loadings separately for spring (Table 2) and summer (Table 3).

In spring, two factors were enough (Table 2 and Fig. 5). The first factor (Factor 1) is related to the temperature change in air and soil at 0 and 1 m. The second factor (Factor 2) determines the strongness of the relationships between RFDs in control and background points and near-surface soil temperature. In spring, there is no significant difference in RFDs between disturbed (control point) and undisturbed (background point) soil layers.

The factor analysis for the summer data (Table 3 and Fig. 6) shows SS loadings > 1 only for Factor 1. Those points of the Factor 1 are the main ones determining RFD in the control point and are caused by temperature change at different soil depths particularly at 0.5 and 1.5 m.

What does the diffusion equation show?

Based on the results of the experiment and its statistical analysis, it was demonstrated that a change in the radon situation can occur when the permafrost conditions in the geological environment change. In the present

experiment, this fact was noticed immediately when the radium source zone thawed. We assume that this is due to the physical properties of ice and permafrost. First of all, it is necessary to take into account the porosity of the ice. This porosity will influence the emanation of the rock. In this case, radon atoms are emanated from the solid phase into the pore space of the soil (production of «free» radon) due to the recoil energy arising from the alpha decay of the parent ²²⁶Ra. It can be assumed that the emanation of rock in its frozen state will be much lower than in the thawed state.

We hypothesized that some hypothetical area is composed of rocks similar to a radium source zone. Distribution of radon concentration in the frozen state and thawed state was calculated up to 10 m deep. The following picture is obtained (Fig. 8).

The following diffusion equation (3) was used to calculate distribution of radon concentration [Marenniy A.M. 2016]:

$$C(x) = C_{Ra} \cdot K_{\text{ЭМ}} \cdot \rho \cdot (1 - e^{-\frac{\lambda}{D} x}) \tag{3}$$

where:

$C(x)$ – distribution function along the vertical profile of the radiation of «free» radon in the rock, Bq·m⁻³;

C_{Ra} – concentration of ²²⁶Ra in the rock, Bq·kg⁻¹;

$K_{\text{ЭМ}}$ – coefficient of radon emanation in soil, stand. units;

ρ – soil density, kg·m⁻³;

λ – radon decay constant, 1·s⁻¹;

D – diffusion coefficient of radon in soil, m²·s⁻¹.

Table 2. Factor analysis from spring data

| Parameters | Uniquenesses | |
|--|--------------|---------|
| Air temp. °C | 0.130 | |
| Soil temp. at 0 m, °C | 0.005 | |
| Soil temp., at 0.5 m, °C | 0.186 | |
| Soil temp., at 1 m, °C | 0.195 | |
| Soil temp., at 1.5 m, °C | | |
| Radon flux density, control point, mBq m ⁻² s ⁻¹ | 0.055 | |
| Radon flux density, background, mBq m ⁻² s ⁻¹ | 0.006 | |
| | Loadings | |
| | Factor1 | Factor2 |
| Air temp. °C | 0.841 | 0.402 |
| Soil temp. at 0 m, °C | 0.833 | 0.549 |
| Soil temp., at 0.5 m, °C | 0.618 | 0.657 |
| Soil temp., at 1 m, °C | 0.778 | 0.446 |
| Soil temp., at 1.5 m, °C | | |
| Radon flux density, control point, mBq m ⁻² s ⁻¹ | 0.500 | 0.834 |
| Radon flux density, background, mBq m ⁻² s ⁻¹ | 0.449 | 0.890 |
| SS loadings | 2.841 | 2.582 |
| Proportion Var | 0.474 | 0.430 |
| Cumulative Var | 0.474 | 0.904 |

Notes: Test of the hypothesis that 2 factors are sufficient. The chi square statistic is 57.95 on 4 degrees of freedom. The p-value is 7.8e-12

Table 3. Factor analysis from summer data

| Parameters | Uniquenesses | |
|--|--------------|---------|
| Air temp. °C | 0.718 | |
| Soil temp. at 0 m, °C | 0.005 | |
| Soil temp., at 0.5 m, °C | 0.129 | |
| Soil temp., at 1 m, °C | 0.264 | |
| Soil temp., at 1.5 m, °C | 0.005 | |
| Radon flux density, control point, mBq m ⁻² s ⁻¹ | 0.028 | |
| Radon flux density, background, mBq m ⁻² s ⁻¹ | 0.994 | |
| | Loadings | |
| | Factor1 | Factor2 |
| Air temp. °C | | 0.529 |
| Soil temp. at 0 m, °C | 0.783 | 0.619 |
| Soil temp., at 0.5 m, °C | 0.925 | 0.128 |
| Soil temp., at 1 m, °C | 0.816 | 0.266 |
| Soil temp., at 1.5 m, °C | 0.998 | |
| Radon flux density, control point, mBq m ⁻² s ⁻¹ | 0.979 | -0.117 |
| Radon flux density, background, mBq m ⁻² s ⁻¹ | - | - |
| SS loadings | 4.088 | 0.770 |
| Proportion Var | 0.584 | 0.110 |
| Cumulative Var | 0.584 | 0.694 |

Notes: Test of the hypothesis that 2 factors are sufficient. The chi square statistic is 38.87 on 8 degrees of freedom. The p-value is 5.2e-06

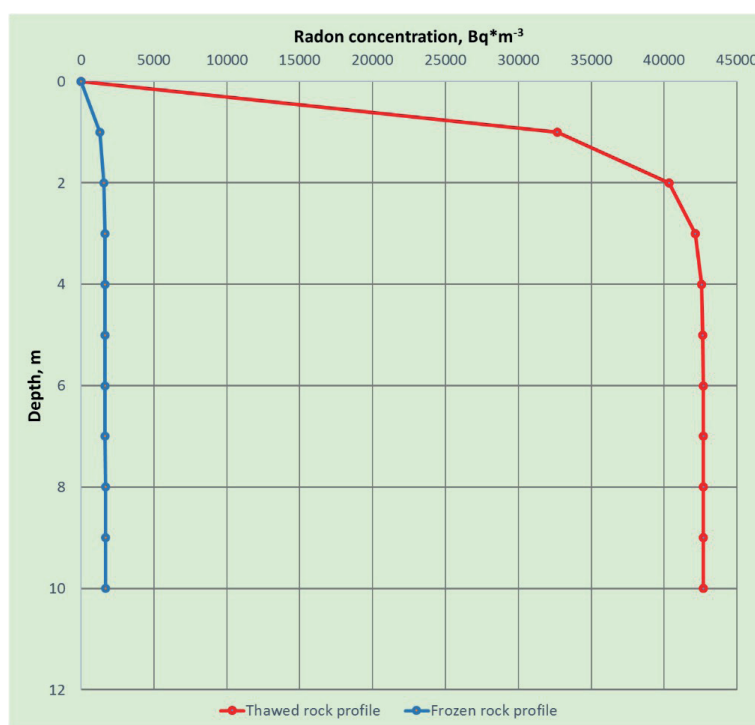


Fig. 8. Distribution of radon concentration in frozen and thawed rocks

The obtained radiation and physical parameters of the radium source zone were used to calculate this diffusion equation. At the same time, for the frozen state, an emanation coefficient equal to 1% was used. This value of the emanation coefficient assumes the absence of radon in a «free» state and its presence in the crystal lattice of ice. Fig. 8 shows that in frozen conditions, the concentration of radon can reach no more than $2000 \text{ Bq}\cdot\text{m}^{-3}$. With the complete thawing of such rocks, the concentration of radon will increase 20 times and can reach $43000 \text{ Bq}\cdot\text{m}^{-3}$. The actual environment and conditions may be completely different. This calculation is shown as a simple example to understand that the condition of permafrost, frozen state of soils and rocks can play a barrier role for radon flux, reducing them by 10-20 times, depending on the characteristics of the frozen rocks (density, porosity). Another fact proving the barrier function of permafrost may be the isotopic ratios in the soil and rock profile up to 20 m deep. For the isotopic ratio, ^{226}Ra and ^{210}Pb can be used. The ratio of these isotopes around 1 would indicate the absence of «movement» of radon, which is most likely in a bound state in the permafrost. This will be included in a future contribution to study the behavior of radon in conditions of frozen ground, permafrost or ice.

Future health risks if the hypothesis is confirmed

The negative impact of radiation exposure on human health is a known fact. The degree of the negative effect of this radiation is determined by the magnitude of the dose regardless if it is caused by natural or artificial source of ionizing radiation (Karabanov 2013, Radon: An Overview of Health Effects 2015). Back in 1988, the Congress of the World Health Organization and the International Agency for Research on Cancer reviewed the available data and recognized that the intake of radon in the body leads to the development of lung cancer in humans (Nenakhova 2006). In 2009, UNSCEAR, based on a detailed scientific assessment of epidemiological data, made a statement at the UN General Assembly that there is direct evidence to support a detectable risk of lung cancer for the population from radon in dwellings. The statement concluded that there is no effective lower threshold of radon concentration below which radon exposure poses no danger. Strong scientific evidence demonstrates that radon-induced lung cancer is a significant public health risk with children at greater risk than adults (as is often the case with exposure to toxic substances/radiation) (Radon indoor air, Canada 2014).

In the case of a hypothesis about the barrier function of permafrost for radon flux, there are theoretical studies with the construction of a mathematical model of radon intake into residential buildings (Glover 2006, Glover 2007, Glover 2022). In these studies, the authors estimated the radon concentration in a residential building in the event of an instantaneous melting of permafrost 13 m thick. According to their calculations, the radon concentration can increase 100 times, which will lead to an excess of the permissible values of the radon concentration (criteria of $100\text{-}300 \text{ Bq}\cdot\text{m}^{-3}$ for many countries). According to the model constructed by the authors, this level can persist for several years and will then gradually decrease. The authors believed this fact is extremely relevant considering the extremely negative effect of radon on the incidence of cancer. Our studies confirm the barrier function of permafrost for radon flux. Based on our measurements, an increase in RFD at the surface up to 20 times is observed.

We assume that residential buildings built without an air layer in permafrost areas may be affected by radon in a warming climate. This will lead to an increase exposure to radon for the people living in such buildings. When confirming this assumption, it will be necessary to provide additional protective actions for such buildings. In addition, it will be necessary to take into account the effect of permafrost thawing when assessing the potential radon hazard of the territory before starting the construction of the new buildings. In Russia, a similar coefficient exists in assessing the potential radon hazard (Klimshin et al. 2010). But the value of that coefficient does not exceed 2. The coefficient takes into account only the layer of seasonal freezing and not the degradation of permafrost. Therefore, it will be necessary to take into account the predictor presented in this work when calling for (amend) existing laws. Such changes in the legislation will prevent a possible negative effect on human health associated with an increase exposure to radon for the population of the Arctic countries. This is especially true for the territories of the central and northern parts of Canada, Russia, the northern part of the Scandinavian (Sweden, Norway, Finland) countries and the United States (Alaska) (Puchkov et al. 2021).

CONCLUSIONS

In this paper, an experiment with a frozen source of radon (red clay with a high content of ^{226}Ra) and its gradual thawing in natural conditions was described. The experiment was carried on a 5-month period with radon and temperature measurements in soil every day. In total, 132 measurements of RFD and soil temperature at different depths were made. These results show a strong relationship between radon flux density and soil temperature profiles at different depths. The calculations of radon sourced from frozen and thawed zones show how temperature phase of substrate (e.g. clays) control the barrier influence of radon migration. From March 1 to July 11, RFD increased 4 times. From the moment the radium source zone began to thaw until its complete thawing, RFD increased by about 7-8 times reaching a maximum value of about $240 \text{ mBq}\cdot\text{m}^{-2}\cdot\text{s}^{-1}$. Fluctuations in RFD after complete thawing of the radium source zone were associated with weather events (rainfalls) and changes in soil characteristics (moisture).

A statistical and factor analysis of the measured values was carried out. There was a good correlation between air and soil temperature ($R=0.73\text{-}0.89$) as well as between RFD in control and background points ($R=0.81$) in March. In May, air temperature and soil temperature at 0 meter ($R=0.85$) were correlated as well as soil temperature at 0 and at 1 meter (0.72). In April, there was no significant correlation in the measured parameters. This is because the RFD variation was only at the beginning of April. After this variation period, the radon activity remained at a constant level. During summer (June), a strong correlation was observed between RFD at the control point and soil temperature at different depths ($R=0.75$ at 0 m, $R=0.79$ at 0.5 m, $R=0.83$ at 1.0 m, $R=0.97$ at 1.5 m). This is because the radium source zone was intensely melting and contributed to an increase in RFD at the surface. Simultaneously, RFD at the background point remained at a constant level and no dependence on soil temperature was found. An increase of 26.7 and $22.2 \text{ mBq}\cdot\text{m}^{-2}\cdot\text{s}^{-1}$ on RFD during spring and summer corresponds to an increase of 1°C of the soil temperature at 1-1.5 m depth.

The factor analysis showed that, in spring, RFD change was mainly caused by air and soil (at 0 and 1 m) temperature

changes. There was a high relationship between RFDs in control and background points and near-surface soil temperatures. In spring, there was no significant difference in RFDs between the soil layers in control and background points. During summer, RFD change was caused by temperature variation at different soil depths, particularly at 0.5 and 1.5 m in the control point.

The calculation of distribution of radon concentration in frozen and in thawed state based on the diffusion equation showed that frozen soils and rocks played a barrier role for radon flux, reducing them by 10-20 times depending on the characteristics of frozen rocks (density, porosity). We

assume that the barrier function of permafrost may be demonstrated further by the study of isotopic ratios of ^{226}Ra and ^{210}Pb in the soil and rock profiles up to 20 m deep. The ratio of these isotopes around 1 would indicate the absence of «movement» of radon, which is most likely in a bound state in the permafrost. This will be the next step in studying the behavior of radon in conditions of frozen ground, permafrost or ice.

The results of the presented experiment confirm the assumption about the barrier function of permafrost for the flow of radioactive radon gas. ■

REFERENCES

- Afonin A., & Korchunov A. (2013). Optimizing block parameters measurements for monitoring radon, thoron and their daughter products in various environments. ANRI, 1, 9-11. (in Russian).
- Aparin B.F., & Sukhacheva E.Yu. (2015). Urban soil classification in the system of Russian and international soil classification. Bulletin of the Soil Institute named after V.V. Dokuchaev, (79), 53-72. (in Russian).
- Arenson L., Colgan W., & Marshall H.P. (2021). Physical, thermal, and mechanical properties of snow, ice, and permafrost. In Snow and ice-related hazards, risks, and disasters, 35-71, DOI: 10.1016/B978-0-12-817129-5.00007-X.
- Baskaran M. (2016). Radon: A tracer for geological, geophysical and geochemical studies (Vol. 367). Basel: Springer.
- Biskaborn B.K., Smith S.L., Noetzi J., Matthes H., Vieira G., Streletskiy D.A., ... & Lantuit H. (2019). Permafrost is warming at a global scale. Nature communications, 10(1), 1-11, DOI: 10.1038/s41467-018-08240-4.
- Buldovicz S.N., Khilimonyuk V.Z., Bychkov A.Y., Ospennikov E.N., Vorobyev S.A., Gunar A.Y., ... & Amanzhurov R.M. (2018). Cryovolcanism on the earth: Origin of a spectacular crater in the Yamal Peninsula (Russia). Scientific reports, 8(1), 1-6, DOI: 10.1038/s41598-018-31858-9.
- Canadian Environmental Law Association. (2014). Radon in indoor air: A review of policy and law in Canada.
- Daraktchieva Z., Wasikiewicz J.M., Howarth C.B., & Miller C.A. (2021). Study of baseline radon levels in the context of a shale gas development. Science of The Total Environment, 753, 141952, DOI: 10.1016/j.scitotenv.2020.141952.
- Egorov V.V., Ivanova E.N., Friedland V.M., & Rozov N.I. (1977). Classification and diagnosis of soils of the USSR. (in Russian).
- Farquharson L.M., Romanovsky V.E., Cable W.L., Walker D.A., Kokelj S.V., Nicolsky D. (2019) Climate Change Drives Widespread and Rapid Thermokarst Development in Very Cold Permafrost in the Canadian High Arctic. Geophysical Research Letters, 46, 12, DOI: 10.1029/2019GL082187.
- Field R.W. (2019). Radon: an overview of health effects.
- Giustini F., Ciotoli G., Rinaldini A., Ruggiero L., & Voltaggio M. (2019). Mapping the geogenic radon potential and radon risk by using Empirical Bayesian Kriging regression: A case study from a volcanic area of central Italy. Science of the Total Environment, 661, 449-464, DOI: 10.1016/j.scitotenv.2019.01.146.
- Glover P.W.J. (2006). Increased domestic radon exposure caused by permafrost thawing due to global climate change, EGU General Assembly, Vienna, Austria, 2-7 April. EGU06-A-01439.
- Glover P.W.J., Blouin M. (2022). Increased Radon Exposure from Thawing of Permafrost Due to Climate Change. Earth's Future, 10, 2, DOI: 10.1029/2021EF002598.
- Glover P.W., & Blouin M. (2007). Modelling increased soil radon emanation caused by instantaneous and gradual permafrost thawing due to global climate warming.
- International atomic energy agency (IAEA) (2013). Measurement and Calculation of Radon Releases from NORM Residues. Technical Reports Series, 474. IAEA, Austria.
- Jensen M.A., Demidov I.N., Larsen E., & Lyså A. (2009). Quaternary palaeoenvironments and multi-storey valley fill architecture along the Mezen and Severnaya Dvina river valleys, Arkhangelsk region, NW Russia. Quaternary Science Reviews, 28(23-24), 2489-2506, DOI: 10.1016/j.quascirev.2009.05.009.
- Ji M., Kong W., Liang C., Zhou T., Jia H., & Dong X. (2020). Permafrost thawing exhibits a greater influence on bacterial richness and community structure than permafrost age in Arctic permafrost soils. The Cryosphere, 14(11), 3907-3916, DOI: 10.5194/tc-14-3907-2020.
- Karabanov A., Zhuk I., Yaroshevich O., Konopelko M., Lukashevich J., & Vasilevsky L. (2013). Radon: health, danger, and protective measures. Science and Innovation, 4(122). (in Russian).
- Klimshin A.V., Kozlova I.A., Rybakov E.N., Lukovskoy M.Yu. (2010). Effect of freezing the surface layer of soil on the radon transport. Vestnik Kamchatskoy regional'noy assotsiatsii «Uchebno-nauchnyy tsentr». Seriya: Nauki o Zemle, 16(2), 146-151. (in Russian with English summary).
- Koptev D.P. (2020). Norilsk spill: lessons and consequences. Drilling and Oil, (7-8), 3-9. (in Russian with English summary).
- Lorenzo-Gonzalez M., Ruano-Ravina A., Torres-Duran M., Kelsey K.T., Provencio M., Parente-Lamelas I., ... & Barros-Dios J.M. (2020). Lung cancer risk and residential radon exposure: A pooling of case-control studies in northwestern Spain. Environmental Research, 189, 109968, DOI: 10.1016/j.envres.2020.109968
- Maier A., Wiedemann J., Rapp F., Papenfuß F., Rödel F., Hehlhans S., ... & Frey B. (2021). Radon Exposure—Therapeutic Effect and Cancer Risk. International Journal of Molecular Sciences, 22(1), 316, DOI: 10.3390/ijms22010316.
- Marenniy A.M., Tsapalov A.A., Miklyaev P.S., Petrova T.B. (2016) Regularities Formation of a Radon Field in the Geological Environment. Pero Publishing House. (in Russian).
- Melnichenko N.A., Tyuveev A.V., Lazaryuk A.Yu, Kustova E.V., & Abramov A.S. (2021). Porosity, permeability and structure of sea ice in Novik Bay (Russkiy Island) according to hydrological measurements, MRI and CT. Bulletin of the Far Eastern Branch of the Russian Academy of Sciences, 1(215), 49-57. (in Russian with English summary).
- Miklyaev P.S., Petrova T.B. (2011) Studies of radon emanation from clays. Water Resources, 38, 868-875, DOI: 10.1134/S0097807811070116.
- Nazintsev Y.L., Panov V.V. (2000). Phase composition and thermophysical characteristics of sea ice. St. Petersburg: Gidrometeoizdat. (in Russian).
- Nenakhova E.V., & Makarov O.A. (2006). Radon and the health of the population. Acta Biomedica Scientifica, (6). (in Russian with English summary).
- Obu J., Westermann S., Bartsch A., Berdnikov N., Christiansen H.H., Dashtseren A., ... & Zou D. (2019). Northern Hemisphere permafrost map based on TTOP modelling for 2000–2016 at 1 km² scale. Earth-Science Reviews, 193, 299-316, DOI: 10.1016/j.earscirev.2019.04.023.

- Payandi-Rolland D., Shirokova L.S., Labonne F., Bénézeth P., & Pokrovsky O.S. (2021). Impact of freeze-thaw cycles on organic carbon and metals in waters of permafrost peatlands. *Chemosphere*, 279, 130510, DOI: 10.1016/j.chemosphere.2021.130510.
- Pereira A., Lamas R., Miranda M., Domingos F., Neves L., Ferreira N., & Costa L. (2017). Estimation of the radon production rate in granite rocks and evaluation of the implications for geogenic radon potential maps: A case study in Central Portugal. *Journal of environmental radioactivity*, 166, 270-277, DOI: 10.1016/j.jenvrad.2016.08.022.
- Petrova T., & Miklyaev P. (2020). Variations of Indoor Radon Concentration in Traditional Russian Rural Wooden Houses. *Radiation Protection Dosimetry*, 191(2), 219-222, DOI: 10.1093/rpd/ncaa156.
- Pokrovsky O.S., Manasypov R.M., Pavlova O.A., Shirokova L.S., & Vorobyev S.N. (2022). Carbon, nutrient and metal controls on phytoplankton concentration and biodiversity in thermokarst lakes of latitudinal gradient from isolated to continuous permafrost. *Science of The Total Environment*, 806, 151250, DOI: 10.1016/j.scitotenv.2021.151250.
- Puchkov A.V., Yakovlev E.Y., Hasson N., Sobrinho G.A., Tsykareva Y.V., Tyshov A.S., ... & Ushakova E.V. (2021). Radon hazard in permafrost conditions: Current state of research. *Geogr. Environ. Sustain*, DOI: 10.24057/2071-9388-2021-037.
- Rodríguez-Martínez Á., Torres-Duran M., Barros-Dios J.M., & Ruano-Ravina A. (2018). Residential radon and small cell lung cancer. A systematic review. *Cancer letters*, 426, 57-62, DOI: 10.1016/j.canlet.2018.04.003.
- Rosenberger A., Hung R.J., Christiani D.C., Caporaso N.E., Liu G., Bojesen S.E., ... & Gomolka M. (2018). Genetic modifiers of radon-induced lung cancer risk: a genome-wide interaction study in former uranium miners. *International archives of occupational and environmental health*, 91(8), 937-950, DOI:10.1007/s00420-018-1334-3.
- Rossiter D.G. (2007). Classification of urban and industrial soils in the world reference base for soil resources (5 pp). *Journal of Soils and Sediments*, 7(2), 96-100, DOI: 10.1065/jss2007.02.208.
- Sabbarese C., Ambrosino F., D'Onofrio A., Pugliese M., La Verde G., D'Avino V., & Roca V. (2021). The first radon potential map of the Campania region (southern Italy). *Applied Geochemistry*, 126, 104890, DOI: 10.1016/j.apgeochem.2021.104890.
- Selvam S., Muthukumar P., Sajeev S., Venkatramanan S., Chung S.Y., Brindha K., ... & Murugan R. (2021). Quantification of submarine groundwater discharge (SGD) using radon, radium tracers and nutrient inputs in Punnakayal, south coast of India. *Geoscience Frontiers*, 12(1), 29-38 DOI: 10.1016/j.gsf.2020.06.012.
- Shirokova L.S., Chupakov A.V., Ivanova I.S., Moreva O.Y., Zabelina S.A., Shutskiy N.A., ... & Pokrovsky O.S. (2021). Lichen, moss and peat control of C, nutrient and trace metal regime in lakes of permafrost peatlands. *Science of the Total Environment*, 782, 146737, DOI: 10.1016/j.scitotenv.2021.146737.
- Syam N.S., Lim S., Lee H.Y., & Lee S.H. (2020). Determination of radon leakage from sample container for gamma spectrometry measurement of ²²⁶Ra. *Journal of environmental radioactivity*, 220, 106275, DOI: 10.1016/j.jenvrad.2020.106275.
- Walter Anthony K., Schneider von Deimling T., Nitze I., Frolking S., Emond A., Daanen R., Anthony P., Lindgren P., Jones B., & Grosse G. (2018). 21st-century modeled permafrost carbon emissions accelerated by abrupt thaw beneath lakes. *Nature Communications*, 9, 3262, DOI: 10.1038/s41467-018-05738-9.
- Yakovlev E., & Puchkov A. (2021). Radon over Kimberlite Pipes: Estimation of the Emanation Properties of Rocks (Lomonosov Diamond Deposit, NW Russia). *Applied Sciences*, 11(13), 6065, DOI: 10.3390/app112411765.
- Zhang Z.Q., Wu Q.B., Hou M.T., Tai B.W., & An Y.K. (2021). Permafrost change in Northeast China in the 1950s–2010s. *Advances in Climate Change Research*, 12(1), 18-28, DOI: 10.1016/j.accre.2021.01.006.
- Zolkos S., Fiske G., Windholz T., Duran G., Yang Z., Olenchenko V., ... & Natali S.M. (2021). Detecting and Mapping Gas Emission Craters on the Yamal and Gydan Peninsulas, Western Siberia. *Geosciences*, 11(1), 21, DOI: 10.3390/geosciences11010021.

APPENDICES

APPENDIX A. STATISTICAL CHARACTERISTICS OF THE OBSERVED PARAMETERS AND CORRELATION MATRICES

| Parameter | Air temp. °C | Soil temp. at 0 m, °C | Soil temp., at 0.5 m, °C | Soil temp., at 1 m, °C | Radon flux density at control point, mBq m ⁻² s ⁻¹ | Radon flux density at background, mBq m ⁻² s ⁻¹ |
|--|--------------|-----------------------|--------------------------|------------------------|--|---|
| March | | | | | | |
| Air temp. °C | 1.00 | 0.89 | 0.81 | 0.73 | 0.48 | 0.38 |
| Soil temp. at 0 m, °C | 0.89 | 1.00 | 0.96 | 0.92 | 0.61 | 0.52 |
| Soil temp., at 0.5 m, °C | 0.81 | 0.96 | 1.00 | 0.96 | 0.66 | 0.60 |
| Soil temp., at 1 m, °C | 0.73 | 0.92 | 0.96 | 1.00 | 0.65 | 0.61 |
| Radon flux density, control point, mBq m ⁻² s ⁻¹ | 0.48 | 0.61 | 0.66 | 0.65 | 1.00 | 0.81 |
| Radon flux density, background, mBq m ⁻² s ⁻¹ | 0.38 | 0.52 | 0.60 | 0.61 | 0.81 | 1.00 |
| April | | | | | | |
| Air temp. °C | 1.00 | 0.46 | 0.16 | 0.23 | 0.02 | 0.02 |
| Soil temp. at 0 m, °C | 0.46 | 1.00 | 0.00 | 0.47 | 0.20 | -0.14 |
| Soil temp., at 0.5 m, °C | 0.16 | 0.00 | 1.00 | 0.19 | -0.16 | -0.28 |
| Soil temp., at 1 m, °C | 0.23 | 0.47 | 0.19 | 1.00 | 0.37 | 0.07 |
| Radon flux density, control point, mBq m ⁻² s ⁻¹ | 0.02 | 0.20 | -0.16 | 0.37 | 1.00 | 0.25 |
| Radon flux density, background, mBq m ⁻² s ⁻¹ | 0.02 | -0.14 | -0.28 | 0.07 | 0.25 | 1.00 |
| May | | | | | | |
| Air temp. °C | 1.00 | 0.85 | -0.10 | 0.43 | 0.42 | 0.32 |
| Soil temp. at 0 m, °C | 0.85 | 1.00 | 0.30 | 0.72 | 0.68 | 0.68 |
| Soil temp., at 0.5 m, °C | -0.10 | 0.30 | 1.00 | 0.64 | 0.78 | 0.82 |
| Soil temp., at 1 m, °C | 0.43 | 0.72 | 0.64 | 1.00 | 0.83 | 0.90 |
| Radon flux density, control point, mBq m ⁻² s ⁻¹ | 0.42 | 0.68 | 0.78 | 0.83 | 1.00 | 0.87 |
| Radon flux density, background, mBq m ⁻² s ⁻¹ | 0.32 | 0.68 | 0.82 | 0.90 | 0.87 | 1.00 |

Table A2. Correlation matrix of parameters in summer

| Parameter | Air temp. °C | Soil temp. at 0 m, °C | Soil temp., at 0.5 m, °C | Soil temp., at 1 m, °C | Soil temp., at 1.5 m, °C | Radon flux density, control point, mBq m ⁻² s ⁻¹ | Radon flux density, background, mBq m ⁻² s ⁻¹ |
|---|-----------------|--------------------------|-----------------------------|---------------------------|-----------------------------|---|--|
| June | | | | | | | |
| Air temp. °C | 1.00 | 0.47 | 0.27 | 0.27 | -0.21 | 0.09 | -0.29 |
| Soil temp. at 0 m, °C | 0.47 | 1.00 | 0.94 | 0.92 | 0.83 | 0.75 | 0.11 |
| Soil temp., at 0.5 m, °C | 0.27 | 0.94 | 1.00 | 0.98 | 0.82 | 0.79 | 0.25 |
| Soil temp., at 1 m, °C | 0.27 | 0.92 | 0.98 | 1.00 | 0.86 | 0.83 | 0.22 |
| Soil temp., at 1.5 m, °C | -0.21 | 0.83 | 0.82 | 0.86 | 1.00 | 0.97 | 0.11 |
| Radon flux density, control point, mBq m ⁻² s ⁻¹ | 0.09 | 0.75 | 0.79 | 0.83 | 0.97 | 1.00 | 0.04 |
| Radon flux density, background, mBq m ⁻² s ⁻¹ | -0.29 | 0.11 | 0.25 | 0.22 | 0.11 | 0.04 | 1.00 |
| July | | | | | | | |
| Air temp. °C | 1.00 | 0.78 | 0.70 | -0.06 | 0.66 | 0.27 | -0.49 |
| Soil temp. at 0 m, °C | 0.78 | 1.00 | 0.80 | -0.04 | 0.80 | 0.08 | -0.42 |
| Soil temp., at 0.5 m, °C | 0.70 | 0.80 | 1.00 | 0.12 | 0.92 | 0.24 | -0.11 |
| Soil temp., at 1 m, °C | -0.06 | -0.04 | 0.12 | 1.00 | 0.40 | 0.88 | 0.39 |
| Soil temp., at 1.5 m, °C | 0.66 | 0.80 | 0.92 | 0.40 | 1.00 | 0.48 | 0.01 |
| Radon flux density, control point, mBq m ⁻² s ⁻¹ | 0.27 | 0.08 | 0.24 | 0.88 | 0.48 | 1.00 | 0.14 |
| Radon flux density, background, mBq m ⁻² s ⁻¹ | -0.49 | -0.42 | -0.11 | 0.39 | 0.01 | 0.14 | 1.00 |

Table A3. Statistical characteristics of the observed parameters

| Parameter | N total | Mean | Stand. Dev. | Min | Med | Max | P10 | P90 |
|--|---------|--------|-------------|--------|--------|--------|--------|--------|
| March | | | | | | | | |
| Air temp. °C | 31 | -5.76 | 7.40 | -22.80 | -4.60 | 4.30 | -14.00 | 3.50 |
| Soil temp. at 0 m, °C | 31 | -2.63 | 3.41 | -8.30 | -3.30 | 3.40 | -6.80 | 2.40 |
| Soil temp., at 0.5 m, °C | 31 | -3.80 | 2.25 | -6.80 | -4.50 | -0.10 | -6.10 | -0.20 |
| Soil temp., at 1 m, °C | 31 | -4.45 | 2.08 | -6.80 | -5.40 | -0.80 | -6.20 | -1.00 |
| Soil temp., at 1.5 m, °C | - | - | - | - | - | - | - | - |
| Radon flux density, control point, mBq m ⁻² s ⁻¹ | 31 | 3.19 | 3.28 | 0.00 | 2.00 | 12.00 | 0.00 | 9.00 |
| Radon flux density, background, mBq m ⁻² s ⁻¹ | 31 | 2.74 | 2.66 | 0.00 | 2.00 | 12.00 | 0.00 | 4.00 |
| April | | | | | | | | |
| Air temp. °C | 30 | 3.50 | 2.95 | -1.90 | 3.40 | 11.00 | -0.10 | 7.65 |
| Soil temp. at 0 m, °C | 30 | 3.91 | 0.90 | 1.20 | 4.05 | 5.30 | 2.85 | 5.10 |
| Soil temp., at 0.5 m, °C | 30 | -0.43 | 0.13 | -0.70 | -0.40 | -0.10 | -0.60 | -0.30 |
| Soil temp., at 1 m, °C | 30 | -0.72 | 0.09 | -0.90 | -0.70 | -0.60 | -0.80 | -0.60 |
| Soil temp., at 1.5 m, °C | - | - | - | - | - | - | - | - |
| Radon flux density, control point, mBq m ⁻² s ⁻¹ | 30 | 15.33 | 2.71 | 11.00 | 15.50 | 22.00 | 12.00 | 18.50 |
| Radon flux density, background, mBq m ⁻² s ⁻¹ | 30 | 14.27 | 1.80 | 10.00 | 14.00 | 18.00 | 12.00 | 16.00 |
| May | | | | | | | | |
| Air temp. °C | 31 | 9.80 | 7.02 | -0.90 | 7.30 | 25.40 | 2.30 | 19.30 |
| Soil temp. at 0 m, °C | 31 | 7.11 | 3.10 | 2.40 | 7.00 | 13.40 | 3.10 | 11.50 |
| Soil temp., at 0.5 m, °C | 31 | 1.29 | 1.99 | -0.60 | -0.10 | 4.50 | -0.40 | 4.20 |
| Soil temp., at 1 m, °C | 31 | -0.40 | 0.23 | -0.80 | -0.40 | 0.00 | -0.70 | -0.10 |
| Soil temp., at 1.5 m, °C | - | - | - | - | - | - | - | - |
| Radon flux density, control point, mBq m ⁻² s ⁻¹ | 31 | 28.19 | 7.12 | 12.00 | 29.00 | 38.00 | 18.00 | 36.00 |
| Radon flux density, background, mBq m ⁻² s ⁻¹ | 31 | 26.58 | 7.44 | 15.00 | 28.00 | 37.00 | 17.00 | 35.00 |
| June | | | | | | | | |
| Air temp. °C | 30 | 16.67 | 3.95 | 8.80 | 17.00 | 23.60 | 11.50 | 21.85 |
| Soil temp. at 0 m, °C | 30 | 13.31 | 2.25 | 8.60 | 13.55 | 16.30 | 9.70 | 15.80 |
| Soil temp., at 0.5 m, °C | 30 | 8.87 | 2.68 | 4.00 | 9.75 | 12.00 | 4.40 | 11.65 |
| Soil temp., at 1 m, °C | 30 | 4.98 | 3.42 | 0.00 | 5.25 | 9.30 | 0.40 | 8.90 |
| Soil temp., at 1.5 m, °C | 20 | 2.43 | 2.26 | -0.10 | 1.95 | 6.30 | 0.05 | 5.95 |
| Radon flux density, control point, mBq m ⁻² s ⁻¹ | 30 | 81.33 | 50.30 | 33.00 | 69.50 | 212.00 | 35.50 | 168.50 |
| Radon flux density, background, mBq m ⁻² s ⁻¹ | 30 | 33.80 | 2.12 | 30.00 | 34.00 | 38.00 | 30.50 | 36.00 |
| July | | | | | | | | |
| Air temp. °C | 10 | 18.76 | 4.53 | 12.30 | 18.50 | 25.50 | 13.45 | 24.75 |
| Soil temp. at 0 m, °C | 10 | 15.73 | 0.84 | 14.20 | 16.10 | 16.40 | 14.25 | 16.40 |
| Soil temp., at 0.5 m, °C | 10 | 13.16 | 0.46 | 12.10 | 13.25 | 13.80 | 12.45 | 13.65 |
| Soil temp., at 1 m, °C | 10 | 8.69 | 0.52 | 8.00 | 8.50 | 9.50 | 8.10 | 9.40 |
| Soil temp., at 1.5 m, °C | 10 | 7.25 | 0.25 | 6.80 | 7.25 | 7.60 | 6.90 | 7.55 |
| Radon flux density, control point, mBq m ⁻² s ⁻¹ | 10 | 213.70 | 20.83 | 185.00 | 217.00 | 241.00 | 185.50 | 238.00 |
| Radon flux density, background, mBq m ⁻² s ⁻¹ | 10 | 33.50 | 2.42 | 29.00 | 34.00 | 36.00 | 29.50 | 36.00 |